A Distributed Model of Ionomeric Polymer Metal Composite

A. Punning,* U. Johanson, M. Anton, A. Aabloo AND M. Kruusmaa

Institute of Technology, Tartu University, Nooruse 1, Tartu 50411, Estonia

ABSTRACT: This article presents a novel model of an ionomeric polymer metal composite (IPMC) material. An IPMC is modeled as a lossy RC distributed line. Unlike other electromechanical models of an IPMC, the distributed nature of our model permits modeling the non-uniform bending of the material. Instead of modeling the tip deflection or uniform deformation of the material, we model the changing curvature. The transient behavior of the electrical signal as well as the transient bending of the IPMC are described by partial differential equations. By implementing the proper initial and boundary conditions we develop the analytical description of the possibly non-uniform transient behavior of an IPMC consistent with the experimental results.

Key Words: IPMC, distributed RC lines.

INTRODUCTION

IONOMERIC POLYMER METAL composites (IPMCs) are materials that bend in electric field (Figure 1). An IPMC actuator consists of a highly swollen ionic polymer sheet, such as Nafion^{TM}, filled with water or ionic liquid and plated with metal on both sides. Applied voltage causes the migration of ions inside the polymer matrix, which in turn causes the non-uniform distribution of the ions inside the polymer. As a result, the polymer sheet bends. The direction of bending depends on the polarity of the applied voltage.

IPMC materials have also sensor properties. When the material is mechanically deformed, it generates a weak voltage between the faces of the IPMC sheet due to the change of the concentration of ions. An overview of the working principle of IPMC actuators and sensors can be found e.g., in Shahinpoor (2003) and Nemat-Nasser and Thomas (2004).

IPMC actuators and sensors have many appealing properties from the implementation point of view. Being noiseless, soft and flexible, mechanically simple, lightweight, and resilient they have potentially many applications in the areas of noise damping, haptics, smart textiles, biorobotics, medicine, space applications and elsewhere (Shahinpoor and Kim, 2005).

The state-of-the-art of the IPMC sensor and actuator technology is not thoroughly understood which makes it difficult to predict the behavior of this material and therefore limits the potential applications areas.

Several models are proposed so far to model the behavior of IPMC sensors and actuators. A systemized overview of the existing models can be found in Kothera (2005). The most accurate IPMC models are derived from first principles and comprise the modeling of underlying electrochemical phenomena coupled to the mechanical bending of the sheet (Asaka and Oguro, 2000; Nemat-Nasser and Thomas, 2004; Tadokoro et al., 2004). While capturing the complex phenomena inside the IPMC actuator those models tend to be complex, computationally time consuming, and require laborious parameter identification.

The empirical models describing the behavior of the actuator on a macro-level are derived experimentally by curve fitting (Kanno et al., 1995; Mallavarapu and Leo, 2001) or based on the description of some sort of an equivalent circuit (Kanno et al., 1996; Newbury and Leo, 2003; Bonomo et al., 2007). Kanno et al. (1996) have proposed a model in a form of an RC-line but by representing the circuit in a form of a first-order transfer function they reduce it to a lumped model and define the relationship between tensile stress and input current. Also, the model proposed by Bao et al. (2002) is based on the assumption of uniform properties but it is recognized that the distributed model would provide a more accurate description. Yim et al. (2006) propose a distributed model, where the IPMC actuator is divided to segments, but each segment is assumed to be driven separately to achieve a waving motion of the actuator and each segment is again treated as a lumped model subject to uniform tensile forces.

The models proposed so far can model the tip displacement or output force of the tip, but not the configuration of the entire actuator surface. The model proposed by us is different in the sense that it takes into consideration the non-uniform deformation of the IPMC material. Figures 1 and 2 represent a typical

*Author to whom correspondence should be addressed.
E-mail: andres.punning@ut.ee

1045-389X/09/00 0001–14 $10.00/0 DOI: 10.1177/1045389X08337170

behavior of the actuator where the bending curvature from the electric contacts along the sheet decreases.

In this article we propose modeling the IPMC actuator as a distributed RC line. This presentation permits identifying the electric current through the polymer matrix at every point of the IPMC sheet. As such, it corresponds more accurately to the real situation where the bending curvature of the actuator at each point is determined by the migration of ions at that particular location. The variations in the ion concentration cause non-uniform bending.

We represent the model of an IPMC actuator in an analytical and simulated form based on the theory of RC transmission lines and show the solution in case of the step input voltage. By coupling the current through the polymer matrix to the mechanical bending of the actuator we derive the electromechanical model of an IPMC. We then proceed by representing the simulation results and thereafter demonstrate that these results are consistent with the experimental data obtained from the experiments of three different types of IPMC.

CHARACTERIZATION OF THE ACTUATOR

Generally, the models of an IPMC described in the literature do not characterize the shape of IPMC-based devices. They usually describe only the motion of the tip or the bending radius of the device assuming that the bending radius is constant. The equipment used to measure these parameters are for instance laser position sensors or force gauges (Jung et al., 2003; Richardson et al., 2003; Bandopadhya et al., 2006).

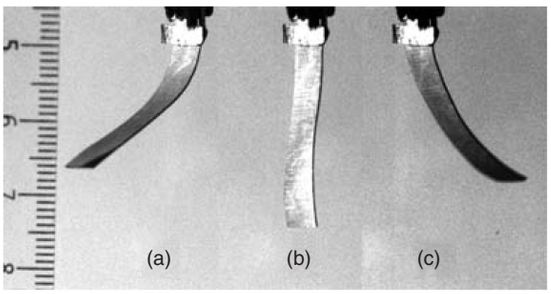

Figure 1. *An IMPC sheet in a bent configuration with the opposite driving voltage polarities (a and c) and in an initial configuration with no electric stimulus applied (b).*

In order to observe the mechanical motion of the actuator, we developed a new methodology that permits describing the flexion of an IPMC. It is a computer vision system consisting of a fast CCD camera and a PC with image processing software. The National Instruments Vision was used for both frame grabbing and image processing. The direction of the camera is set transverse to the actuator and the experiment is illuminated from the background through a frosted glass. In perfect conditions the image of the actuator recorded in such a way consists of a single contrast curved line. It is easy to use image processing software to process the shape frame by frame. The separate frames of a bending actuator combined on one image for bending and on the other image for relaxation, are depicted in Figure 2.

It is apparent from Figure 2, that in the beginning of the input pulse (images 0–0.4 s in Figure 2(a)) the actuator bends sharply near the input contacts only, the free end remains almost straight.

Later (images 0.4–1.0 s in Figure 2(a)) the flexion of the actuator propagates gradually on, but at the region close to the contacts does not increase any more. During the relaxation (images 1.0–4.0 s in Figure 2(b)) the sharp decrease of the flexion takes place close to the input contacts again, whereas the remaining part of the actuator straightens slowly in a few seconds.

The voltage drop along the electrodes of the actuator can be recorded by attaching additional terminals to its surface. The outline of the experimental setup for electrical measurements is depicted in Figure 3.

We measure the voltage distribution on the surface of a working IPMC-based actuator or sensor by attaching a set of pairs of lightweight contacts to its surface using special clips, and connect them via thin wires to the measuring equipment. Voltages U_C, U_D, U_E, and U_F

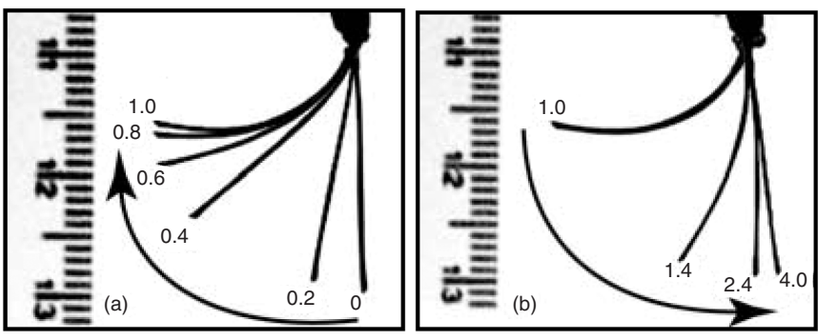

Figure 2. *Overlay of a series of frames showing the response of an actuator to a 1s driving voltage pulse: (a) actuation during the pulse; (b) relaxation after the pulse. The numeric characters indicate the time instant of the frame.*

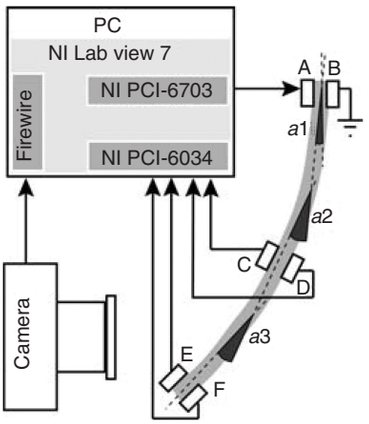

Figure 3. *Setup for electrical measurements.*

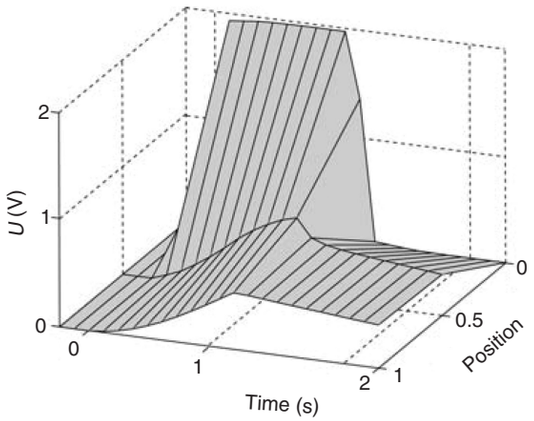

Figure 4. *Voltages along a bending actuator. The 'Position' axis stands for the relative coordinate starting from the input contacts.*

with respect to the ground are measured at the contacts C, D, E, and F, respectively. The input voltage U_A is measured at the contact A. The voltages between the two faces of the sample can be calculated as $U_C - U_D$ and $U_E - U_F$.

The voltages measured on an actuator, with a bending similar to bending in Figure 2, are represented as a 3D graph in Figure 4.

It is apparent from Figure 4 that even in the middle of the sample the voltage does not reach a substantial value. The voltage at the free end only slightly differs from the voltage in the middle.

In order to describe the bending movement of the actuator, the image of the bending sheet is divided into segments, assumed having a constant curvature. The principle of determining the bending angles is shown in Figure 3 (angles $a1 - a3$). The bending angles of the segments are calculated from each frame of the video. Figure 5 depicts the transformation of the bending angles of the actuator, electrically characterized in Figure 4. It shows that the flexion of the sheet is faster and stronger close to the input contacts, getting

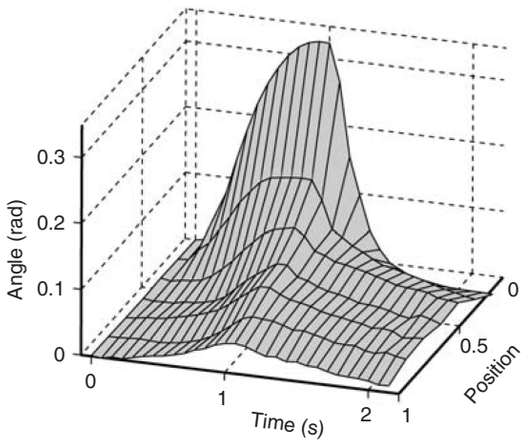

Figure 5. *Mechanical response of an actuator to a step input voltage.*

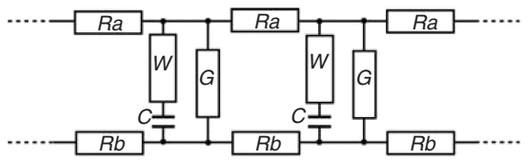

Figure 6. *The distributed RC line describing an IPMC, represented by a series of equivalent circuits with discrete elements.*

progressively weaker as well as delayed towards the free end of the sample.

It is apparent that the two graphs – the graph of voltages versus position and time (Figure 4), and the graph of bending angles versus position and time (Figure 5) – are similar. The characteristic behavior of both – voltage and bending angles – is delayed and progressively weakening towards the position axis.

A DISTRIBUTED MODEL OF IPMC

The fact that the electrical perturbation as well as the change of the flexion spread along the actuator at finite speed and the fact that the flexion and voltage along the surface behave similarly, were the motivations to develop a distributed model of an IPMC.

The basis of the model is the distributed model of an IPMC proposed by Kanno et al. (1996). Originally, Kanno divided a piece of an IPMC into ten similar segments and modeled the relation between the input current and the tip displacement. By dividing the same piece into an infinite number of infinitesimally short similar segments, we have an RC transmission line. The resulting distributed RC line can be represented by a series of equivalent circuits with discrete elements as shown in Figure 6. The transient behavior of electrical signals – voltage, electric current, and charge – along these kind of lines can be described by partial

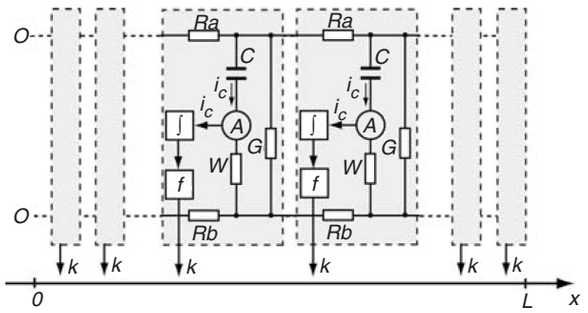

Figure 7. *The distributed model of an IPMC.*

differential equations (PDE) with the proper initial and boundary conditions.

The distributed model of an IPMC represented by an infinite series of equivalent circuits with discrete elements of infinitesimally short single units is given in Figure 7. The conductivity of the electrodes of an IPMC is represented by a series of resistances of the opposite electrodes *Ra* and *Rb*, connecting the single units. Each single unit contains the electrical parameters determining the propagation of voltage along the transmission line and the elements for calculating the mechanical behavior of the actuator within the limits of that unit.

There are two fundamental causes of the electric current between the electrodes of an IPMC through the polymer matrix:

(1) The material is ion conductive. Relocating ions constitute the pseudocapacitance of the double-layer, which forms at the interface between the ion exchange membrane and the metal electrode (Sadeghipour et al., 1992). As described above, the resulting irregular density of possibly solvated mobile ions is the cause of bending of the IPMC. The resulting deformation of the IPMC is proportional to the total amount of relocated ions. In the equivalent circuit the pseudocapacitance is modeled by shunt capacitors C between the electrodes in each unit. The conductivity W denotes the summarized transversal ionic conductivity of the electrodes and the ionomer.
(2) The current caused by electrochemical electrode reactions, for example electrolysis of the solvent. The electrode reactions appear only if the voltage between the electrodes exceeds some certain critical level, which depends on the materials used. The electrode reactions consume energy and affect the propagation of voltage, but do not have a direct effect on the deformation of the IPMC. In the equivalent circuit the electrode reactions are represented as shunt resistors G between the electrodes in each single unit.

The electric charge $q(x,t)$ determines the bending angle $k(x,t)$ within the limits of the single unit. As the electric charge can be expressed as the derivative of the current with respect to time, the total electric charge $q(x,t)$ carried over within each unit is calculated as an integral of current $i_C(x,t)$. Figuratively, each single unit of the RC distributed line contains a block composed of an ammeter, measuring current $i_C(x,t)$ through the capacitance C, an integrator in order to determine the charge moved over within the limits of that unit, and function f describing the bending effect of a charge, moving to the electrode. In the simplest case the bending angle is proportional to the charge and the block f contains:

$$k(x,t) = \Upsilon q(x,t), \tag{1}$$

where Υ is defined as the coefficient for the bending effect of the charge.

THE ANALYTICAL EQUATIONS DESCRIBING THE DISTRIBUTED MODEL OF AN IPMC

When the input current is applied through one end of a circuit as shown in Figures 6 or 7, the current flows through $C-W$ and G of the whole chain. According to Ohm's Law, the current induces voltage drops on the resistances *Ra* and *Rb* and the voltage across the line diminishes until the circuit reaches an equilibrium state. In the course of charging of the capacitive elements C the voltages and currents change, but at every time instant the system stays in its equilibrium state. This transient behavior can be described by PDEs.

The step response of a system is the output of the system when a unit step function is used as the input and it is a common analysis tool used to determine certain metrics about a system. As we show hereinafter, the step response of the distributed line depicted in Figure 6 is solvable in an analytical form. On the other hand it is easy to verify the theoretical model by applying the step voltage to the input of the IPMC actuators, describing their electromechanical response and measuring the transient behavior of the electrical parameters.

In this section we give the equations describing the transient behavior of the voltage $u(x,t)$ for the distributed line of the finite length L shown in Figure 6 when a voltage step is applied to its input. The derivation of the PDE and the procedure of applying the initial and boundary conditions is described in detail in (Punning and Jalviste, 2009) and is based on the solution of the heat equation with different boundary conditions (Powers, 2006; Kreyszig, 2006). From the analytical solution describing the transient behavior of voltage we derive the transient behavior of the charge $q(x,t)$

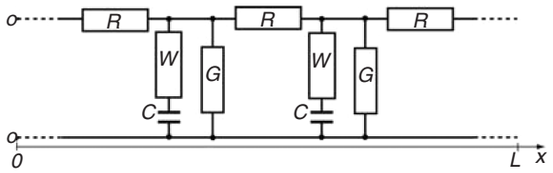

Figure 8. *The Cauer canonical form of the line represented in Figure 6.*

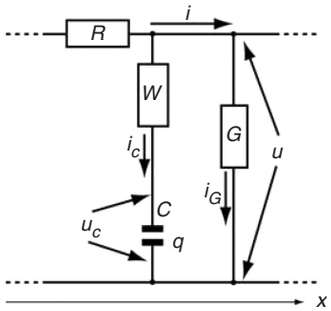

Figure 9. *The meaning of the line parameters, voltages, and currents for the distributed line.*

of the capacitive element C, actually determining the amount of bending of IPMC, for example in the simplest case following the Equation (1).

First, we transfer the line shown in Figure 6 into the *Cauer canonical form* (Szekely, 2003) by replacing the two resistances Ra and Rb by their sum $R = Ra + Rb$. The resulting line is presented in Figure 8.

As shown in Figure 9, the parameters R and C are the resistance of the conductive layer and the capacitance of the dielectric per unit length of the line, respectively. The loss parameters W and G are the transversal conductivities per unit length along the line. For visual clarity of Figure 9 the parameters R, C, G, and W, all defined per unit length along the coordinate x, are represented as discrete elements of a single cell of the line. The voltage checkpoints and the selected positive directions of the currents are indicated by arrows. We assume that all these parameters are uniform and time-invariant. Voltages and currents are assumed to be functions of the distance along the line and time, i.e., $i \equiv i(x,t)$, $i_C \equiv i_C(x,t)$, $i_G \equiv i_G(x,t)$, $u \equiv u(x,t)$, and $u_C \equiv u_C(x,t)$.

The Behavior of Voltage

The variation of current along the coordinate x at instant t is equal to the sum current through the chains '$C - W$' and 'G':

$$\frac{\partial}{\partial x} i(x,t) = -(i_C(x,t) + i_G(x,t)), \tag{2}$$

where

$$i_G(x,t) = Gu(x,t). \tag{3}$$

The variation of voltage along the coordinate x is equal to the voltage drop on resistance R:

$$\frac{\partial}{\partial x} u(x,t) = -Ri(x,t). \tag{4}$$

Current $i_C(x,t)$ charging the capacitance C is given by:

$$i_C(x,t) = C\frac{\partial}{\partial t} u_C(x,t). \tag{5}$$

Voltages in the chain $C - W$ add up to the line voltage:

$$u(x,t) = u_C(x,t) + \frac{1}{W} i_C(x,t). \tag{6}$$

We now have four equations with four unknown variables: $i(x,t)$, $i_C(x,t)$, $u_C(x,t)$, and $u(x,t)$. After some substitutions and rearrangements we get the PDE describing the transient behavior of voltage $u(x,t)$ along the line in the form:

$$\frac{\partial^3}{\partial x^2 \partial t} u(x,t) + \frac{W}{C}\frac{\partial^2}{\partial x^2} u(x,t) - R(W+G)\frac{\partial}{\partial t} u(x,t) - \frac{RGW}{C} u(x,t) = 0. \tag{7}$$

This equation can be easily solved by a method called the separation of variables. The general solution of the PDE (7) for $u(x,t)$ is:

$$u(x,t) = (A\sin(\omega x) + B\cos(\omega x))e^{-\frac{W(\omega^2+RG)}{C(\omega^2+RG+RW)}t}, \tag{8}$$

where A and B are arbitrary constants, with values determined from the boundary conditions.

Next, we introduce the term *steady voltage distribution*. After a long time ($t \to \infty$) under a constant input voltage the capacitance C finally charges completely and the voltages $u(x,t)$ and $u_C(x,t)$ are equalized, $u(x) = u_C(x)$. As it can be inferred form Figures 8 and 9, the steady current through the distributed resistive network, formed by R and G, still remains. This results in a diminishing steady voltage, denoted by $u_{ST}(x)$, along the line. The equation describing the steady voltage distribution is:

$$\frac{\partial^2}{\partial x^2} u_{ST}(x) = RGu_{ST}(x). \tag{9}$$

By applying the condition of the input voltage U at $x = 0$: $u_{ST}(0) = U$, and the open end condition,

$i_{ST}(L) = 0$ or $(\partial/\partial x)u_{ST}(L) = 0$, to its general solution $u_{ST}(x) = Ae^{\sqrt{RG}x} + Be^{-\sqrt{RG}x}$, we find that:

$$u_{ST}(x) = U\frac{\cosh(\sqrt{RG}(x-L))}{\cosh(\sqrt{RG}L)}. \tag{10}$$

It is self-evident that when the input of the initially charged line is shorted, the capacitance C finally discharges through the resistive network and the shorted input, and the steady voltage is zero: $u_{ST}(x) = 0$.

The initial/boundary conditions can be applied to the Equation (8) using the method of Fourier series. This procedure is thoroughly described in Punning and Jalviste (2009). Naturally, it is possible to define many different initial/boundary conditions to (8), that result in an analytical solution. In the current article we describe only two distinct cases of practical importance:

(A) The step voltage with amplitude normalized to 1 is applied to the input of the initially discharged line. The initial and boundary conditions for this case are:

  (a) initial voltage distribution: $u(x,0) = 0$
  (b) input voltage at $x = 0$: $u(0,t) = 1$
  (c) open end condition: $(\partial/\partial x)u(L,t) = 0$
  (d) steady voltage distribution: $u_{ST}(x) = (\cosh(\sqrt{RG}(x-L))/\cosh(\sqrt{RG}L))$

(B) The shorted input of the line been under the input voltage of a unit amplitude until the steady distribution is formed. The initial and boundary conditions for this case are:

  (a) initial voltage distribution: $u(x,0) = (\cosh(\sqrt{RG}(x-L))/\cosh(\sqrt{RG}L))$
  (b) input voltage at $x = 0$: $u(0,t) = 0$
  (c) open end condition: $(\partial/\partial x)u(L,t) = 0$
  (d) steady voltage distribution: $u_{ST}(x) = 0$

In general, the voltage-step response of the distributed lines of length L depicted in Figure 8 can be expressed as:

$$u(x,t) = U\sum_{n=1}^{\infty}(b_n\varphi(\omega_n x)e^{-k_n t}) + u_{ST}(x), \tag{11}$$

where:

$$k_n = \frac{W(\omega_n^2 + RG)}{C(\omega_n^2 + RG + RW)}, \tag{12}$$

and where $\varphi(\omega_n, x)$, ω_n, b_n, and $u_{ST}(x)$ are the eigenfunctions, the eigenvalues, the Fourier coefficients, and the steady voltage distribution, respectively. All these quantities depend on the initial/boundary conditions. Applying the boundary conditions for our two cases, we get that the solutions for voltage are:

$$\text{(A)}\quad u(x,t) = \sum_{n=1}^{\infty}\left(-b_n\sin\left(\frac{2n-1}{2L}\pi x\right)e^{-k_n t}\right) + \frac{\cosh(\sqrt{RG}(x-L))}{\cosh(\sqrt{RG}L)} \tag{13}$$

$$\text{(B)}\quad u(x,t) = \sum_{n=1}^{\infty}\left(b_n\sin\left(\frac{2n-1}{2L}\pi x\right)e^{-k_n t}\right) \tag{14}$$

where:

$$k_n = \frac{W(4RGL^2 + \pi^2(2n-1)^2)}{C(\pi^2(2n-1)^2 + 4RL^2(G+W))} \tag{15}$$

and

$$b_n = \frac{4\pi(2n-1)}{\pi^2(2n-1)^2 + 4RGL^2}. \tag{16}$$

The Behavior of Charge

As described above, the bending angle of the actuator $k(x,t)$ is determined by the transitory charge $q(x,t)$ of the capacitance C. The PDE describing the behavior of the charge can be derived similar to the derivation of the PDE for voltage in the previous section. Using the relation describing that the current through the capacitor is the derivative of its charge by time:

$$i_C(x,t) = \frac{\partial}{\partial t}q(x,t) \tag{17}$$

and the relation between the charge and voltage of a capacitor is:

$$u_C(x,t) = \frac{1}{C}q(x,t), \tag{18}$$

It is possible to convert the Equations (2)–(6) to four new equations with four unknown variables: $i(x,t)$, $i_C(x,t)$, $q(x,t)$, and $u(x,t)$. From these equations it is possible to derive the PDE describing the behavior of the charge $q(x,t)$:

$$\frac{\partial^3}{\partial x^2\partial t}q(x,t) + \frac{W}{C}\frac{\partial^2}{\partial x^2}q(x,t) - R(W+G)\frac{\partial}{\partial t}q(x,t) - \frac{RGW}{C}q(x,t) = 0. \tag{19}$$

It is intriguing that the PDEs describing the behavior of voltage (7) and the charge (19) are exactly similar. The only difference between these two is in the initial and boundary conditions. The general solution for the charge $q(x,t)$ is similar to (8):

$$q(x,t) = (A\sin(\omega x) + B\cos(\omega x))e^{-\frac{W(\omega^2+RG)}{C(\omega^2+RG+RW)}t}. \quad (20)$$

Nevertheless it is not possible to apply the initial/boundary conditions to (20) using the method of separation of the variables, because the charge $q(0)$ at the boundary $x = 0$ is not a constant but some unknown time-dependent function.

Instead, we derive the behavior of the charge $q(x,t)$ from the Equation (6). Using the relations (17) and (18), we can write:

$$u(x,t) = \frac{1}{C}q(x,t) + \frac{1}{W}\frac{\partial}{\partial t}q(x,t). \quad (21)$$

Solving (21) for $q(x,t)$ gives:

$$q(x,t) = \left(\int_0^t Wu(x,\tau)e^{\frac{W}{C}\tau}d\tau + \rho(x)\right)e^{-\frac{W}{C}t}, \quad (22)$$

where $\rho(x)$ is the constant of integration. From the boundary conditions we can find that $\rho(x)$ equals to the initial distribution of charge corresponding to the initial voltage distribution at $t = 0$. For the case (A) the initial distribution of charge is self-evidently zero: $\rho(x) = 0$. For the case (B) the initial charge $q_{ST}(x)$ can be found from the final steady voltage distribution of the case (A) as:

$$\rho(x) = Cu_{ST}(x), \quad (23)$$

where $u_{ST}(x)$ is defined by (10).

After substituting the behavior of voltage described by (13) or (14) and the corresponding steady charge distribution into (22) we get the behavior of the charge $q(x,t)$ along the line for our two cases.

Hydraulic Pressure

The bending movement of an IPMC is produced by the hydraulic pressure caused by the moving (possibly solvated) charged particles. In the simplest case the amount of matter carried over by the migrating cations is proportional to the charge, see (1):

$$k(x,t) = \Upsilon q(x,t),$$

where Υ is defined as the coefficient for the bending effect of the charge.

Several authors have described the slow back-relaxation of the IPMC actuators after the quick response to the applied voltage (Bao et al., 2002; Shahinpoor, 2003). This phenomenon is explained with the leakage of solvent resulting from a high-pressure layer near the cathode toward to the anode through channels in the polymer backbone. The research of relaxation effect and the development of the equations for the hydraulic pressure considering the back-relaxation, suitable for the distributed model of an IPMC, is one of the subjects of our future work.

Bending Radius

The derivation of the relation between the curvature of the swollen polymer matrix and the charge carried over is described in Berry and Pritchet (1984). The equations are derived similar to those employed by Timoshenko (1925) in his work on bi-metallic strips. Actually, Berry and Pritchet describe the method of determining the coefficient of moisture swelling of polymers by their bending curvature. In our PMC model we use the result conversely – we determine the bending curvature from the non-uniform concentration profile of the solute of possibly solvated ions and solvent inside the polymer.

Assuming that the polymer is isotropic and swells in volume V proportionally to a uniform concentration η_0 of the solute, we can write:

$$\varepsilon = K\eta_0, \quad (24)$$

where ε is a hygroscopic strain analogous to a thermal expansion strain of bi-metal thermostats, and K is a linear swelling parameter equal to one-third of the volumetric swelling factor:

$$K = \eta_0 \frac{1}{3}\frac{\Delta V}{V}. \quad (25)$$

A non-uniform concentration profile of solute $\eta(z,t)$ through the strip will cause elongation (Figure 10), bending and internal stress. With the assumption that plane cross-sections remain planar, the stress $\sigma(z,t)$ is given by

$$\frac{\sigma(z,t)}{E_1} = K\eta(z,t) - \varepsilon_0(t) - \frac{z}{r(t)}, \quad (26)$$

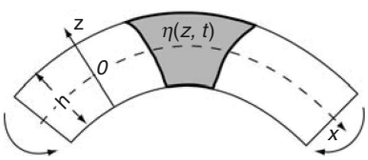

Figure 10. *Self-induced bending of a polymer strip caused by the concentration profile $\eta(z,t)$ of the solute through the polymer layer.*

where E_1 denotes $E/(1-v)$, E and v are Young's modulus and Poisson's ratio of the polymer layer, respectively, $\varepsilon_0(t)$ is the strain at middle plane $z=0$, and $r(t)$ is the radius of curvature. Since there are no external forces acting on the polymer layer, we can write:

$$\frac{1}{r(t)} = \frac{12K}{h}\int_{-1/2}^{1/2} \eta(s,t)\mathrm{d}s, \tag{27}$$

where we introduced the dimensionless coordinate $s = z/h$ for convenience.

Assuming that the concentration profile of solute along the z-coordinate of the strip is linear: $\eta(x,s,t) = s\mu(x,t)$, Equation (27) reduces to:

$$r(x,t) = \frac{h}{K\mu(x,t)}. \tag{28}$$

The Behavior of Electric Current

The distribution of electric current between the surface electrodes of an IPMC sample cannot be directly measured. Nevertheless, it can be derived from the previous equations. As described in 'A Distributed Model of IPMC' section, it can be derived by analyzing the effects of its components to the bending motion. The current caused by ionic conductivity $i_C(x,t)$, described by (17), is related to the behavior of charge $q(x,t)$, actually producing the movement. The current caused by electrochemical electrode reactions $i_G(x,t)$, described by (3), only consumes energy but does not cause the bending motion. Both components of the current jointly determine the distribution of voltage and the charge and hence, the bending movement of the actuator.

The total input current $i_{in}(t)$ of the sample is determined by all currents over the full length of the distributed line:

$$i_{in}(t) = \int_0^L (i_C(x,t) + i_G(x,t))\mathrm{d}x. \tag{29}$$

ESTIMATION OF THE PARAMETERS

The values of the resistances of the surface electrodes of an IPMC can be measured using a four-probe system. This method eliminates inexactnesses caused by the inconsistent current density and the resistances of the contacts.

The values of the parameters G, W, and C can be determined using a technique with voltage step pulses as follows. A small piece of an IPMC material is fixed between contact clamps made of gold so that the whole piece of the measured material is covered with the contacts. In this configuration the resistance of the electrodes does not influence the results. The typical response of electric current corresponding to a long-lasting step voltage input is presented in Figure 11. Electric current peaks sharply at the very first moment (at instant A). After charging the whole pseudo-capacitor, electric current remains at a stable level (at instant B).

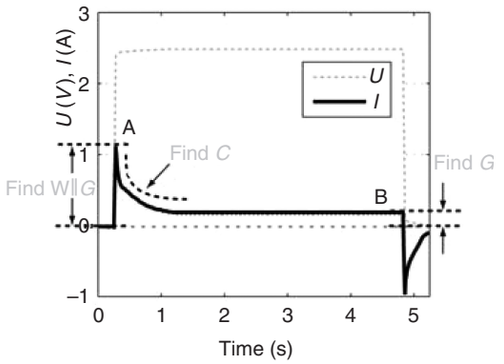

Figure 11. *Response of the electric current to a rectangular voltage pulse.*

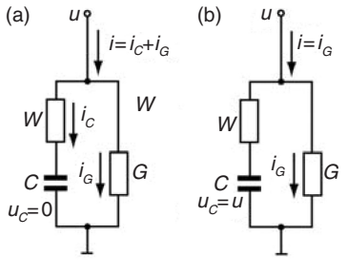

Figure 12. *Estimation of the resistances G and W.*

This behavior of current can be explained by analyzing the equivalent circuit illustrated in Figure 12. At the very first moment, when the capacitor C is totally discharged, the current flows through the parallel resistances G and W (instant A). When the capacitance C is totally charged, the current flows through resistance G only (instant B). The capacitance C can be found from the decay of the electric current.

VERIFICATION OF THE MODEL

In order to prove the validity of the distributed model of the IPMC, we present the actual behavior of different IPMC actuators and the computational results of the simulations using the equations given above. First we compare the behavior of the two fundamentally different IPMC materials, then the actuators made of the same material, but having different dimensions.

Table 1. The parameters of the samples.

Sample	Dimensions (mm)	Thickness of ionomer (μm)	Ra (Ω/cm)	Rb (Ω/cm)	W (1/Ω·cm)	G (1/Ω·cm)	C (F/cm)	Cations
1	10 × 35	250	9	5	1	0.0005	0.02	Li^+
2	10 × 35	180	0.5	0.5	0.015	0.0001	0.02	EMI^+
3	8 × XX[a]	180	3	1.5	0.5	0.0015	0.05	Li^+

[a]The length of the Sample 3 is variable: 47 mm, 32 mm, and 25 mm.

We used the following IPMC samples for experimental validation:

Sample 1 – an IPMC covered with platinum electrodes using the method of electroless deposition;
Sample 2 – an IPMC covered with gold electrodes using the direct assembly method described in Akle (2007).
Sample 3 – IPMC material Musclesheet™ provided by Biomimetics Inc in 2004. It is a proprietary ionic polymer film covered with platinum electrodes.

The parameters of the samples, measured using the methodology described in 'Estimation of the Parameters' section, are given in Table 1.

Behavior of Actuators with Different Electrical Parameters

The experiments show that the electromechanical responses of the different types of IPMCs are different. Some materials bend faster, some slower; some have almost constant bending radius, some bend non-uniformly. In order to demonstrate the validity of the distributed model of the IPMC for different materials, we compare the results of the experiments carried out with two fundamentally different IPMC materials manufactured by us and the simulations of the distributed model of the IPMC using the estimated parameters. We give the parameters of the samples of both measured materials using the methodology described in 'Estimation of the Parameters' section, and present the graphs of voltage and bending movement as described in 'Characterization of the Actuator' section. Simultaneously, we simulate the same graphs by the equations given in 'The Analytical Equations Describing the Distributed Model of an IPMC' section using the measured parameters and compare the measured and simulated behaviors of the samples.

The Sample 1 is made of 0.25 mm thick Nafion membrane and covered with platinum electrodes using the method of electroless deposition. It is a water-containing IPMC, intended to work in a wet environment. The cations introduced to the ionomer were Li^+. This material is thick, hence more stiff than Sample 2. Thicker material contains potentially more cations, thus it has a relatively large pseudocapacitance. The resistance of the electrodes of this sample is rather high, but still good enough to ensure conductivity. The non-uniform behavior of this sample is considerable due to the high resistance of the electrodes. The value of the conductivity W (Figure 7) is relatively high. When the applied voltage is lower than the voltage required for the electrolysis of water (the value of G) is very low – in the range of about 10^4 per Ω cm. When the applied voltage is close to the voltage required for water electrolysis, the conductivity G increases sharply up to about 10^1 per Ω cm.

Due to the high conductivity W and the relatively high resistance of the electrodes Ra and Rb, the non-uniform behavior of the Sample 1 is more evident than that of the Sample 2.

The experimental results of the voltage measurements and the electromechanical response of the Sample 1 are depicted in Figures 4 and 5, respectively.

The simulation results of the Sample 1 are given in Figure 13. The graphs demonstrate that voltage increases rapidly close to the input contacts and more slowly further away from the input contacts (Figure 13(a)).

As mentioned above, it is not possible to measure the distribution of electric current through the sheet directly. This data can be only derived from the simulations, using the Equation (17). The distribution of current depicted in Figure 13(b) produces the bending motion of the sample presented in Figure 13(c). The graph shows that the actuator moves sharply only close to the input contacts. The noticeably weaker curvature change of the free end appears after a short delay. The behavior of voltage and the bending angles are rather similar to the parameters obtained by the measurements of a real actuator. They are presented in Figures 4 and 5, respectively.

Sample 1 exhibits insistent back-relaxation, half second after the beginning of the input pulse already as seen from Figure 5. As we have no model for relaxation yet, we give here only the graphs for our case (A) – the step voltage is applied to the input of the initially discharged actuator.

Sample 2 is an IPMC made of 0.18 mm thick Nafion membrane containing ionic liquid. It is covered by a thin layer of RuO_2 powder and 20 nm gold foil electrodes

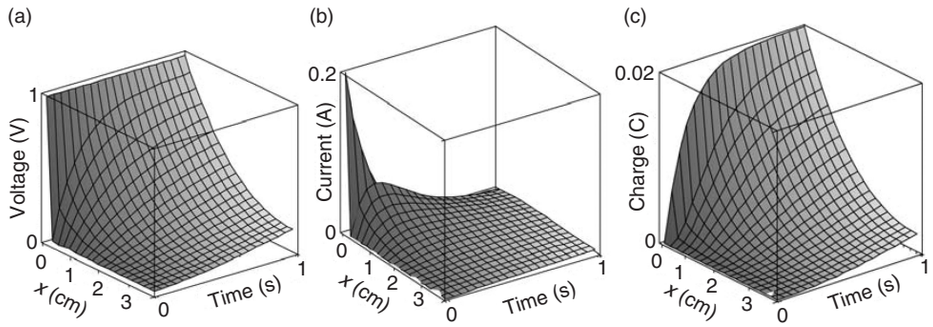

Figure 13. *Simulations of Sample 1: (a) voltage, (b) current, (c) charge.*

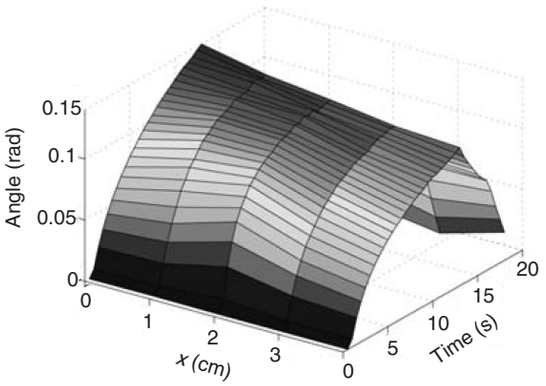

Figure 14. *Measured mechanical response of Sample 2.*

glued to the ionomer with the dilution of Nafion. This material is intended to work in air. The conductivity of the surface of the gold electrodes of that material is very high; however, the poor conductivity of the RuO_2 layer between the gold foil and the ionomer causes a high value of W. The large surface area of the RuO_2 powder supposedly creates large pseudocapacitance of the IPMC material. The ionic liquid used was 1-ethyl-3-methylimidazolium trifluoromethanesulfonate and the cations introduced to the polymer were EMI^+.

Due to the poor conductivity of the RuO_2 layer between the gold electrode and the ionomer the ionic current inside the ionomer cannot grow fast. For that reason the voltage drop along the electrodes is imperceptible and the IPMC has nearly a constant bending radius as depicted in simulations in Figure 14.

As electric current between the electrodes cannot grow, this IPMC is slow. It gains its maximal flexion in minutes.

Sample 2 bends slowly with an almost uniform bending radius over its full length. During the pulse the voltage along the sample is distributed nearly uniformly so that the voltage drop occurs on the conductivity W.

Figure 15 depicts the simulations of the charge calculated according to (22) when voltage is applied and at the time of relaxation after shorting of the input contacts.

The distribution of current between the surface electrodes is presented in Figure 15(b). In contrast to Sample 1 where the current peaked only for a very short time near the contacts creating non-uniform bending; the current of the Sample 2 is several orders of magnitudes weaker, but remains almost uniform along its full length for a long time, thereby producing uniform bending.

The Behavior of Actuators of Different Lengths

The length L of the IPMC actuators is one of the parameters of the model. According to Equations (13), (14), and (22), the transient behavior of the IPMC actuators is different for the actuators having different length. The transient flexion of a shorter actuator is not just similar to the first part of the longer one. In order to compare the behavior of the actuators of different lengths, we recorded some experiments of the flexion of a strip of an IPMC, cut it shorter, and repeated the experiment. This method ensures that the electrical parameters of the strips are the same. The IPMC material used in these experiments is the Sample 3.

For all experiments, the driving signal of the IPMC is a 2 V rectangular pulse. The overlays of a series of frames are represented in Figure 16. It is clearly visible that the bending of the long actuator is inert and weak (Figure 16(a)), while the bending of the free tip of the almost twice shorter actuator (Figure 16(c)) is much sharper and higher.

The photos of the strips of the IPMC are depicted in Figure 17.

Figure 18 depicts the simulated transient behavior of charge of the actuators of different lengths, calculated according to Equation (22). According to (1) the graphs of the transient flexion are similar, but have different vertical scale. The graphs exhibit that the amplitude of flexion of the shorter actuator is higher and it is gained earlier than that of the longer actuators.

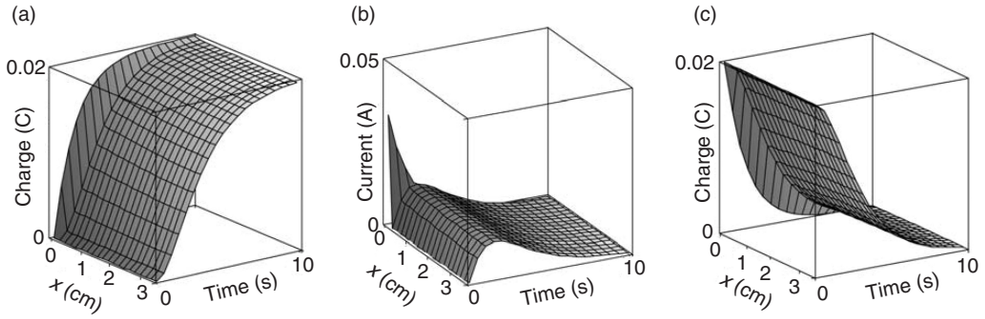

Figure 15. *Simulations of Sample 2. (a) charge during the step voltage input; (b) current during voltage input; (c) charge during relaxation.*

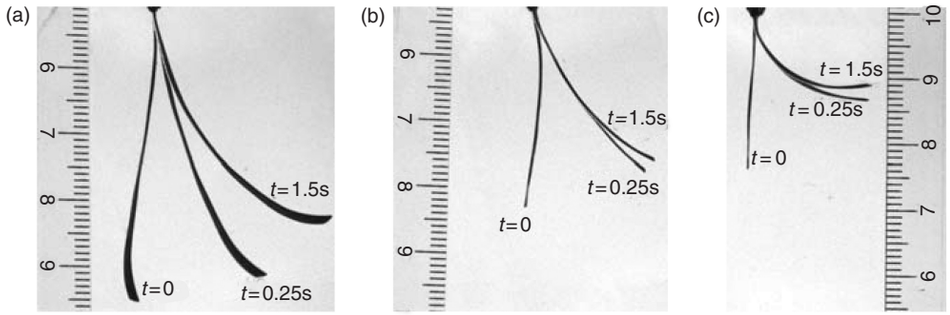

Figure 16. *Overlay of a series of frames at different time instants in three experiments with actuators made of the same material – Sample 3. The time instants of the frames are the initial position (t = 0 s); in the middle of the bending (t = 0.25 s); and the steady position (t = 1.5 s).*

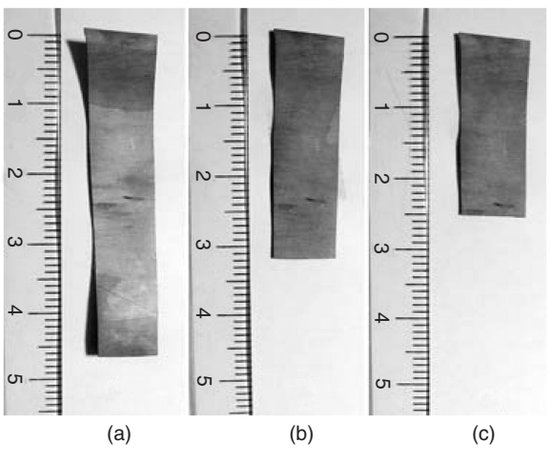

Figure 17. *IPMC actuators of different lengths. A short slice is cut off from the same piece to obtain the next actuator.*

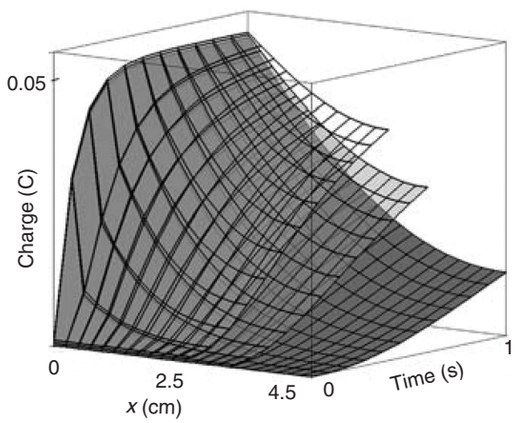

Figure 18. *Simulated transient behavior of the charge of IPMC actuators of different lengths made of the same IPMC material.*

Quantitative Validation of the Model

DETERMINATION OF THE EMPIRIC CONSTANT Υ

As explained above, the bending angle of an actuator at any location is proportional to the charge carried over at that particular location. The coefficient for the bending effect of the charge Υ (see (1)) is the only empirical constant in the model. It is reasonable to assume that Υ is constant all over the actuator if the experiments are done within a short period of time (i.e., the solvation level of the sample does not change considerably). With this assumption, we can identify Υ for the specific actuator for an arbitrary $k(x, t)$, and use the obtained value for the remaining points of the surface or even in the

subsequent experiments. For model validation, the parameter Υ can be determined by comparing the experimental graph $k(x,t)$ and the simulated graph $q(x,t)$ of the mechanical response of the actuator. The obtained value holds for the whole actuator for a while, as long as the material will not get mechanically exhausted or desolvated.

Error Estimation

There are two sets of parameters that are determined experimentally, both are possible sources of measurement errors:

(1) the determination of the bending angles, see 'Characterization of the Actuator' section and Figure 3;
(2) the estimation of the electrical parameters *Ra*, *Rb*, *G*, *W*, and *C* of the material, see 'Estimation of the Parameters' section.

As the description of the shape of the actuator in time-domain is obtained by image processing, we should estimate the error of bending angles from the pixel sizes of the image of the actuator. Due to the setup of our camera and optics the width of the image of the actuator is as few as 1–2 pixels. For a segment of 60 pixels long, the largest error of the bending angle is $2/60 = \pm 8\%$. This error is not cumulative as each segment is treated separately. The smaller the segment is, the better it describes the shape of the actuator, but the larger is the measurement error.

The electrical parameters were estimated with series of measurements (at least 200 each), and by averaging over the measurements. The standard deviation of the measurements was <5% for all cases. When the measurements were performed at low voltages and electric currents, the results did not depend on the actual values of the voltages and currents.

VALIDATION OF THE MODEL WITH ERROR ESTIMATES

As described above, the largest measurement error comes from the measurements of the bending angles. In order to validate the model quantitatively we depict the error corridor of the angle measurements and the simulated results with the obtained electrical parameters on the same diagram. Figure 19 shows results for this comparison for Samples 1 and 2. The arrow shows the conditions at which the coefficient Υ is determined: $x = 0$, $t = 0.8\,\mathrm{s}$ for Sample 1 and $x = 0$, $t = 8\,\mathrm{s}$ for Sample 2.

We have chosen to identify Υ at the contacts of the actuator (at $x = 0$), where we presume that the possible measurement error is smallest because of the large bending angle. We found that $\Upsilon = 0.28/0.019 = 14.7$ for Sample 1 and $\Upsilon = 0.13/0.02 = 6.5$ for Sample 2. For Sample 3 (Figures 15 and 18) $\Upsilon = 5.4$.

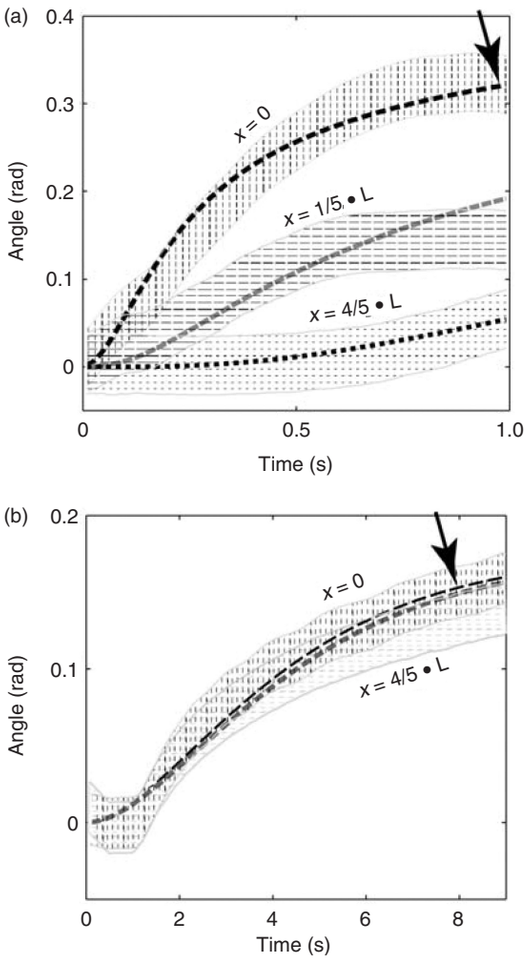

Figure 19. *Comparison of the experimental and simulated results. (a) Sample 1, (b) Sample 2. The diagrams represent the error corridors of the measured bending angles at different positions in conjunction with the simulated graphs (dashed lines). The arrow shows the conditions at which the coefficient Υ is determined.*

The diagrams indicate that even if the electrical parameters vary in the range of the measurement error, the simulated graph remains in the error corridor of the measured bending angles as long as the back-relaxation will not occur. The dissimilarity between the simulated and experimental behavior is clearly recognizable e.g., in Figure 19(a), where the actuator relaxes at the position $x = 1/5 \cdot L$ at $t > 0.8\,\mathrm{s}$. As our model does not describe back-relaxation, this dissimilarity starts to become evident and increases in time.

DISCUSSION

The distributed 1D model of an IPMC presented in this article consists of a number of lumped models coupled with a spatial parameter – a generally uneven distribution of voltage caused by the resistance of the electrodes. It shows a good correlation with the experimental data obtained from the measurements conducted with different IPMC materials. Its advantages with respect to the previous models are:

- it permits modeling the non-uniform flexion of the IPMC actuator in spatial and time domain;
- it permits modeling large flexion of the IPMC material;
- it takes into account the real measurable parameters of the material – resistance of the electrodes and capacitance. Apart from the previously developed models it does not reduce it to a uniform lumped model;
- it is scalable, i.e., the length of the actuator is one of the parameters of the model;
- the values of the measurable parameters – the capacitance of the material, the resistance of the electrodes and the length – may vary on a large scale.

The described model gives the analytical solution for the free bending of the IPMC actuators only. It does not take into account the mechanical parameters of IPMC membranes, for example the viscoelasticity of polymer membranes, the blocking force produced by the IPMC actuator, inertia, etc. Presumably the combination of the electrical distributed model and the theory of mechanics of multilayer elastic thin films would give a result, capable of expressing the force produced by an arbitrary segment of the actuator.

The described analytical model presumes that the electrical parameters of the material: Ra, Rb, G, W, and C are invariant. This presumption is valid at low voltages only. Measuring the resistances G and W with voltage pulses of various amplitudes gives a well-determined relation between the values of the resistors and the voltage. When the amplitude of the voltage approaches to the voltage required for water electrolysis, the resistances G and W decrease fast due to the electrode reactions, reaching very low values. In this case the analytical equations given in 'The Analytical Equations Describing the Distributed Model of an IPMC' section are not tenable any more.

We assume that the proposed model is also applicable to the IPMC sensors. According to (7) the voltage at the output contacts of a sensor depends on time and distance between the bending area and the output. If the deformation is continuous or distributed, the values of $u(x, t)$ should be superpositioned. Verification of the proposed model for IPMC sensors is a subject of our future work.

ACKNOWLEDGMENTS

This work is supported by Estonian Ministry of Education, European Science Foundation, Estonian Science Foundation grants 6765, 6785 and 6763, U.S. CRDF Grant No. 16049 and by Estonian Information Technology Foundation.

REFERENCES

Asaka, K. and Oguro, K. 2000. "Bending of Polyelectrolyte Membrane-platinum Composites by Electric Stimuli. Part II, Response Kinetics," *J. Electroanal. Chem.*, 480:186–198.

Akle, B. et al. 2007. "Direct Assembly Process: A Novel Fabrication Technique for Large Strain Ionic Polymer Transducers," *J. Mater. Sci.*, 42:7031–7041.

Bandopadhya, D. et al. 2006. "Active Vibration Suppression of a Flexible Link Using Ionic Polymer Metal Composite," In: *Proc. IEEE Conference on Robotics, Automation and Mechatronics*, pp. 1–6, Bangkok.

Bao, X. et al. 2002. "Measurements and Macro Models of Ionomeric Polymer-metal Composites (IPMC)," In: *EAPAD Conference 2002, Proc. SPIE*, Vol. 4695, pp. 286-293, San Diego, CA.

Berry, B.S. and Pritchet, W.C. 1984. "Bending-cantilever Method for the Study of Moisture Swelling in Polymers," *IBM J. Res. Develop.*, 28(6):662–667.

Bonomo, C. et al. 2007. "A Nonlinear Model for Ionic Polymer Metal Composites as Actuators," *Smart Mater. Struct.*, 16:1–12.

Jung, K. et al. 2003. "Investigations on Actuation Characteristics of IPMC Artificial Muscle Actuator," *Sens. Act. A: Phys.*, 107(2):183–192.

Kanno, R. et al. 1995. "Modeling of ICPF Actuator, Modeling of Electrical Characteristics," *Proc. IEEE 21st Intl Conf. on Industrial Electronics, Control, and Instrumentation*, Vol. 2, pp. 913–918.

Kanno, R. et al. 1996. "Linear Approximate Dynamic Model of an ICPF Actuator," In: *Proc. IEEE Intern. Conf. on Robotics and Automation*, Vol. 1, pp. 219–225, Minneapolis.

Kothera, C.S. 2005. "Characterization, Modeling, and Control of the Nonlinear Actuation Response of Ionic Polymer Transducers," PhD Dissertation, Dept. of Mechanical Engineering, Virginia Tech.

Kreyszig, E. 2006. *Advanced Engineering Mathematics*, 9th edn, Wiley, New York.

Mallavarapu, K. and Leo, D. 2001. "Feedback Control of the Bending Response of Ionic Polymer Actuators," *J. Intell. Mater. Syst. Struct.*, 12(3):143–155.

Nemat-Nasser, S. and Thomas, C.W. 2004. "Ionomeric Polymer–metal Composites," In: Bar-Cohen, Y. (ed.), *Electroactive Polymer (EAP) Actuators as Artifical Muscles. Reality, Potential, and Challenges*, p. 171, SPIE Press, Washington.

Newbury, K. and Leo, D. 2003. "Linear Electro-mechanical Model of Ionic Polymer Transducers – Part I: Model Development," *J. Intell. Mater. Syst. Struct.*, 14(6):333–342.

Punning, A. and Jalviste, E. 2009. "Analytical Solution for Voltage-step Response of Lossy Distributed RC Lines," *IEEE Trans. Microw. Theory Tech.*, 57(2):449–457.

Powers, D.L. 2006. *Boundary Value Problems and Partial Differential Equations*, Elsevier.

Richardson, R.C. et al. 2003. "Control of Ionic Polymer Metal Composites," *IEEE/ASME Trans. Mech.*, 8(2):245–253.

Sadeghipour, K. et al. 1992. "Development of a Novel Electrochemically Active Membrane and "Smart" Material Based Vibration Sensor/Damper," *Smart Mater. Struct.*, 1:172–179.

Shahinpoor, M. 2003. "Ionic Polymer-conductor Composites as Biomimetic Sensors, Robotic Actuators and Artificial Muscles – A Review," *Electrochim. Acta*, 48:2343–2353.

Shahinpoor, M. and Kim, K.J. 2005. "Ionic Polymer–metal Composites: IV. Industrial and Medical Applications," *Smart Mater. Struct.*, 14:197–214.

Tadokoro, S. et al. 2004. "Modeling IPMC for Design of Actuation Mechanism," In: Bar-Cohen, Y. (ed.), *Electroactive Polymer (EAP) Actuators as Artifical Muscles. Reality, Potential, and Challenges*, SPIE Press, Washington.

Timoshenko, S.P. 1925. "Analysis of Bi-metal Thermostats," *J. Opt. Soc. Am.*, 11:233–255.

Yim, W. et al. 2006. "Dynamic Modeling of Segmented Ionic Polymer Metal Composite (IPMC) Actuator," In: *Proc. IEEE/RSJ Int. Conf. on Intelligent Robots and Systems*, pp. 5459-5464, Beijing, China.